Microstructural Analysis of Corrosion Inhibition in sub-100-nm-Scale Josephson Circuits

M. I. Faley, M. Arzeo, T. Denneulin, A. Kovács, G. Ummethala, A. H. Tavabi, O. Mukhanov, *Fellow, IEEE*, and R. E. Dunin-Borkowski

***Abstract*—We have studied nanobridge Josephson junctions (nJJs) and nJJ-based circuits using microstructural analysis and measurements of electron transport properties to reveal the possible origins of a spread in superconducting parameters (T_c, I_c, etc.) and long-term stability. The structures were prepared by dc magnetron sputtering from Nb, Ti and TiN targets, with electron beam exposure of HSQ resist and reactive ion etching in pure SF_6 gas. Microstructural characterization was performed using aberration-corrected scanning transmission electron microscopy imaging and elemental mapping using energy-dispersive X-ray spectroscopy. The distributions of elements in nanostructures based on Ti-Nb-Ti heterostructures and TiN films were compared. Oxygen-free TiN nJJs are of interest for the realization of corrosion-resistant superconducting circuits, including qubits with operating temperatures down to 10 mK. Ti-Nb-Ti heterostructures contain oxygen that has been chemisorbed by the Ti layers and are intended primarily for operation at 4.2 K. Superconducting through-silicon vias between circuits on opposite sides of a wafer can be realized by using direct writing of superconducting current leads with focused-ion-beam-induced deposition of superconducting films. Particular emphasis is paid to the inhibition of oxygenation and corrosion on the nanometer scale by using new materials and methods, which promise to bring superconducting chip manufacture closer to circular-economy-related objectives. Our work helps to realize the large-scale integration of superconducting circuits that have long-term stability, including nanoSQUIDs, qubits and classical superconducting digital circuits, such as Single Flux Quantum based circuits.**

***Index Terms*—Nanolithography, nanobridge josephson junctions, corrosion, titanium nitride, transmission electron microscopy, through-silicon vias.**

I. Introduction

CURRENTLY, gate-based quantum processors are becoming increasingly complex, and after 2033 they are planned to be able to run fault-tolerant circuits containing a billion gates on 2000 logical qubits [1], [2]. In order to enable such quantum computing systems and to provide fast, low-latency feed-back for real-time error correction at low-power dissipation, the qubit control electronics should be placed at low temperature in close proximity to the qubits. This situation can be realized by using energy-efficient single-flux-quantum (SFQ) superconducting control electronics integrated on multichip modules, or by making use of the back side of the processor's wafer with superconducting through-silicon vias (TSVs) [3], [4]. Such a system configuration would benefit from the compatibility of Josephson junctions used for qubits and SFQ control electronics. Moreover, the increased number of Josephson junctions and their density on chips creates incentives for the miniaturization of superconducting circuits, which has not improved significantly over the past 15 years. One reason for this stagnation apparently lies in the chosen materials [5].

Modern superconducting classical and quantum circuits are typically based on superconductor-insulator-superconductor (SIS) Josephson junctions, with an AlO_x tunnel barrier that has an area of over $(100\,\text{nm})^2$ and superconducting electrodes, which are typically made of Nb or Al [6], [7]. Dielectric losses in the AlO_x tunnel barrier suppress the coherent state of the qubits due to coupling with two-level system (TLS) defects residing in the tunnel junction. They scale as $A_J{}^2/C$, where A_J is the tunnel junction area and C is the total capacitance [8], [9]. A smaller Josephson junction area and dielectric-free structures with minimized interfaces between different materials would therefore be beneficial for qubit coherence.

In SIS junctions, the critical current density depends exponentially on oxide thickness. All subsequent fabrication steps are therefore limited to temperatures of $<200\,^\circ\text{C}$. This limitation has an impact on fabrication options for scaling multi-layer SFQ circuits to higher integration densities, which can be helped by employing interlayer dielectric processing at $>400\,^\circ\text{C}$. Josephson junctions that are capable of withstanding higher temperature fabrication processes are desired.

An additional problem is aging of Al and Nb films. Aging of Josephson junctions with Al electrodes is a problem that can be partially eliminated by applying a "bandage" layer and passivation in an oxygen atmosphere [7]. However, Al corrodes quickly: as a measure of its corrosion resistance, Al films are etched away in a few seconds even by a standard resist developer containing 2% TMAH. Nb films are more stable and can be held in the same developer for $\sim$1 day. Nb is susceptible to corrosion

Received 6 January 2026; revised 29 January 2026; accepted 29 January 2026. Date of publication 6 February 2026; date of current version 17 February 2026. This work was supported in part by European Union as part of the Horizon Europe Call HORIZON-INFRA-2021-SERV-01 under Grant 101058414 and co-funded by U.K. Research and Innovation (UKRI) through the U.K. Government's Horizon Europe funding guarantee under Grant 10039728, in part by the Swiss State Secretariat for Education, Research and Innovation (SERI) under Contract 22.00187, and in part by ReMade DOI: 10.3030/101058414. *(Corresponding author: M. I. Faley.)*

M. I. Faley, T. Denneulin, A. Kovács, G. Ummethala, A. H. Tavabi, and R. E. Dunin-Borkowski are with the ER-C-1, Forschungszentrum Jülich GmbH, 52428 Jülich, Germany (e-mail: m.faley@fz-juelich.de).

M. Arzeo and O. Mukhanov are with the SEEQC, 80146 Naples, Italy.

Color versions of one or more figures in this article are available at https://doi.org/10.1109/TASC.2026.3661936.

Digital Object Identifier 10.1109/TASC.2026.3661936

due to its reaction with O_2 and H_2O in laboratory air. Oxygen penetrates downwards along grain boundaries in columnar Nb films, forming Nb_2O_5 crystallites that expand and crack the Nb films [10], [11], and [12]. This behavior affects both quantum and classical superconducting circuits by increasing rf losses, creating TLSs, increasing susceptibility to flux trapping, and reducing integrated circuit reliability.

The aging of Josephson junctions, which is greater for smaller junctions, can be reduced significantly by choosing an appropriate corrosion-resistant material. Nb nanostructures (nanobridges) can be fabricated using electron beam lithography (EBL) [13], but relatively rapid degradation of their superconducting properties is observed when they are exposed to air at 1 bar pressure. Much better corrosion resistance has been observed for TiN nanobridge Josephson junctions (nJJs) [14], [15]. TiN is known for its applications in super hard, corrosion resistant and decorative coatings. Films of TiN are CMOS compatible and are used in semiconducting microelectronics to create ohmic contacts to Si, anti-diffusion barrier layers and biocompatible implants [16].

The replacement of three-layer Josephson junctions with nJJs resolves the problem of dielectric losses in the AlO_x tunnel barrier, simplifies the technology by reducing the number of layers and lithography stages, allows for a more than tenfold reduction in size, and eliminates use of a dirty lift-off process. In addition to lower dielectric losses, qubits that are based on nJJs can be less sensitive to charge noise and, in turn, can have longer dephasing times [17].

In the present work, we describe the preparation of TiN nJJs and their chemical analysis using energy dispersive X-ray (EDX) spectrometry on the nm scale. The distributions of elements in nJJs based on Ti-Nb-Ti heterostructures and TiN films are compared. Superconducting TSVs between circuits on opposite sides of a wafer are realized by using direct writing of superconducting current leads with focused-ion-beam-induced deposition of superconducting films.

II. Experimental Details

Samples were prepared on 200-µm-thick Si substrates, which were buffered on both sides by low-stress 100-nm-thick SiN films. The substrates were cleaned in acetone, propanol, and deionized water before being placed in a homemade sputtering machine and evacuated to $<10^{-7}$ mbar base pressure using oil-free pumps. TiN films with thicknesses of 10 to 20 nm were deposited at a heater temperature of 700°C (∼550°C substrate temperature) at a rate of ∼3 nm/min from 50-mm-diameter 99.95 % pure TiN target using pulsed reactive DC magnetron sputtering. Deposition was performed in an Ar(90%)-N_2(10%) gas mixture at a total pressure of 0.01 mbar. For the stated purity of Ar and N_2 gases of 99.9999 %, the possible O_2 contamination was below 10^{-10} mbar. Before deposition, additional degassing of the chamber and cleaning of the TiN target were carried out under deposition conditions by pre-sputtering onto a closed shutter for over 10 minutes.

For nanoscale patterning of TiN films, EBL with 2% hydrogen silsesquioxane (HSQ) resist (XR-1541-002) and reactive ion etching (RIE) with SF_6 gas were used. The resist thickness and its electron beam exposure dose were 30 nm and 3 mC/cm^2, respectively. Resist development was carried out in 25 % TMAH for 15 s in an ultrasonic bath, followed by rinsing in running deionized water for 1 min. Residuals of resist were removed in ∼2 s in a buffered HF (BHF) solution, followed by rinsing in deionized water.

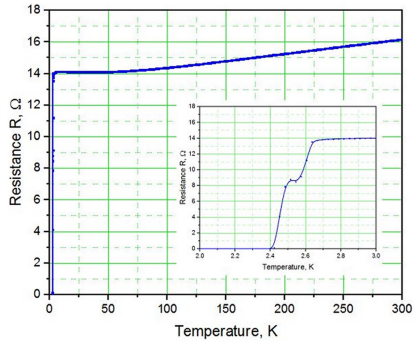

Fig. 1. *R(T)* dependence of a 20-nm-thick TiN film grown at a heater temperature of 700°C. The inset shows the *R(T)* dependence at the superconducting transition.

A Quantum Design (QD) Physical Property Measurement System (PPMS) DynaCool was used to electrically test the nJJs at temperatures between 1.7 and 300 K. Au contact pads on a Pt sublayer were deposited using metal shadow masks and magnetron sputtering.

The preparation of ∼50-nm-thick lamellae for scanning transmission electron microscopy (STEM) measurements was carried out using a Xe plasma focused ion beam (PFIB) thermo fisher scientific (TFS) Helios Hydra DualBeam system. The same system was used for etching holes in the 200-µm-thick Si wafers and direct focused ion beam induced deposition of superconducting stripes of W.

An FEI Titan G2 80-200 ChemiSTEM aberration-corrected TEM was used for the observation of microstructure and elemental distribution in cross-sections of TiN nJJs down to the atomic scale [18], [19]. Spectrum imaging using STEM high-angle annular dark-field (HAADF) imaging and EDX spectroscopy was used to create maps of the spatial distribution of elements at high spatial resolution. EDX maps were processed using TFS Velox software.

III. Results

The superconducting transition temperature T_c of TiN films decreases with decreasing film thickness and deposition temperature. Whereas a 700-nm-thick film deposited at a heater temperature of 930°C has $T_c \approx 5.25$ K [14], a 20-nm-thick film deposited at 700°C has $T_c \approx 2.4$ K (see Fig. 1).

The coherence length ξ is smaller in thinner films $\sim \sqrt{\xi d}$, where d is the film thickness, but diverges near the transition to the superconducting state, taking values of ∼50 nm at 2 K and ∼20 nm at 10 mK for TiN films. This dependence provides the opportunity to realize nJJs whose dimensions are smaller than the coherence length, which is necessary to realize Josephson

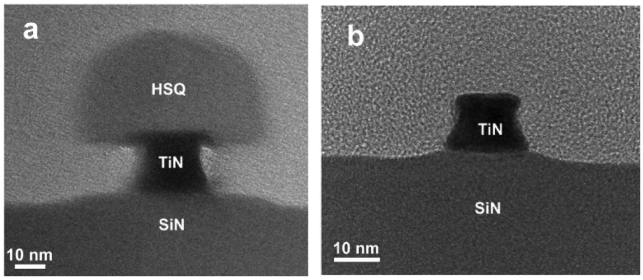

Fig. 2. Cross-sectional TEM images of TiN nJJs (a) coated with HSQ mask residues and (b) after removal of HSQ mask residues using BHF.

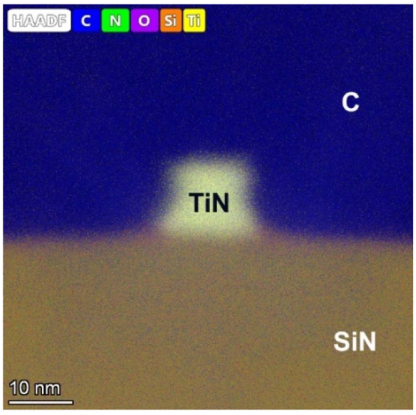

Fig. 3. Cross-sectional HAADF STEM image with superimposed elemental maps of C, N, O, Si, and Ti measured using STEM/EDX spectrum imaging for a TiN nJJ.

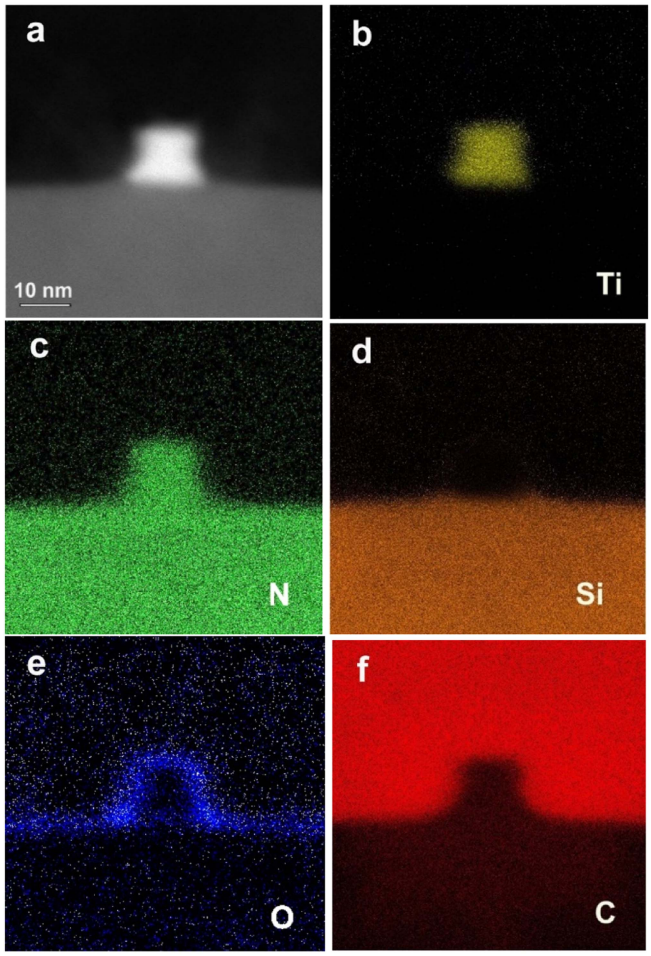

Fig. 4. (a) Cross-sectional HAADF STEM image and elemental maps of (b) Ti, (c) N, (d) Si, (e) O, and (f) C extracted from TEM/EDX spectrum imaging of a TiN nJJ.

behaviour in nJJs [20]. By varying the film thickness, the deposition temperature, and the nJJ width, the nJJ parameters can be tuned to the values that are required for a wide range of classical and quantum superconducting circuits.

After RIE, residuals of the HSQ mask with an undercut in the TiN film were observed, as shown in the form of a bright-field (BF) TEM image in Fig. 2(a). The undercut is proportional to the film thickness and is approximately 2 times smaller for a film thickness of 10 nm.

The standard method of removing resist residue using an oxygen plasma is not effective because HSQ resist is not made from pure hydrocarbons, but is a cross-linked network structure of Si and O atoms [21]. In this case, a buffered HF (BHF) solution works better, and is harmless to TiN films: neither the microstructure nor the superconducting properties (T_c and I_c) of TiN nJJ junctions are changed after such a removal of HSQ resist (see Fig. 2(b)), demonstrating the chemical inertness and corrosion resistance of TiN nJJs. A protective C layer was used to prepare lamellae for cross-sectional TEM measurements.

Figs. 3, 4 and 5 show the result of spectrum imaging performed by simultaneously recording EDX spectra and STEM images. Elemental maps of a TiN nJJ are combined with an HAADF STEM image in Fig. 3. A cross-sectional HAADF STEM image and maps of (b) Ti, (c) N, (d) Si, (e) O, and (f) C in a TiN nJJ are shown in Fig. 4(a)–(f). No O was detected in the TiN nJJ. O observed above the nJJ likely results from adsorption from air before deposition of the C protection layer during lamella preparation.

For comparison, cross-sectional EDX maps of a Ti-Nb-Ti nJJ that was used for nanoSQUIDs in our previous work [22] is shown in Fig. 5. Here, a significant amount of O was observed in the Ti layer: Ti acts as a getter material and absorbs O from gas residues in the chamber during sputtering.

An important milestone for the future integration of TiN nJJs into superconducting and semiconductor classical and quantum circuits has been reached: superconducting TSVs have been realized using Xe PFIB technology (see Figs. 6 and 7). The highest Si etch rate of $\sim$1000 μm^3/min is achieved for a current of the Xe^+ focused ion beam of $\sim$2.5 μA. By using Xe PFIB irradiation and $W(CO)_6$ precursor gas, stripes of tungsten carbide (W-C) with an enhanced critical temperature $T_c \approx 5.6$ K were deposited. It took $\sim$30 min to make a hole with a shallow edge and an additional 30 min to deposit the superconducting stripe. The use of PFIB eliminates standard TSV preparation steps, such as chemical etching, lithography and atomic layer deposition. The TFS Helios Hydra DualBeam system used here allows for the automated production of multiple TSVs. A TiN film can be fabricated on both sides of a Si wafer by chemical vapor

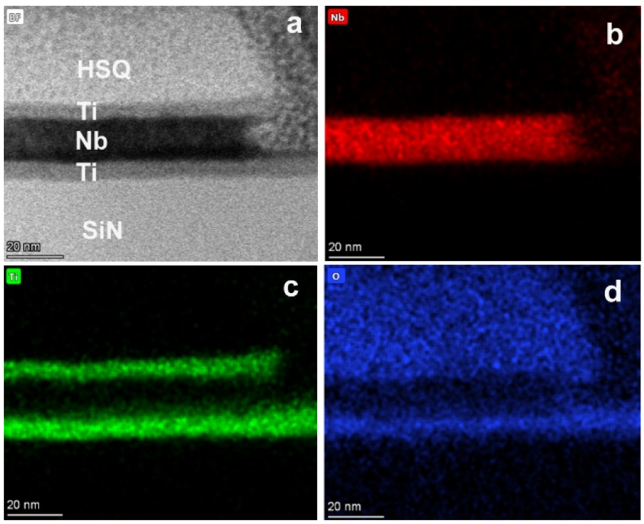

Fig. 5. (a) Cross-sectional BF STEM image and maps of (b) Nb, (c) Ti, and (d) O extracted from STEM/EDX spectrum imaging of the Ti-Nb-Ti nJJ described in [22].

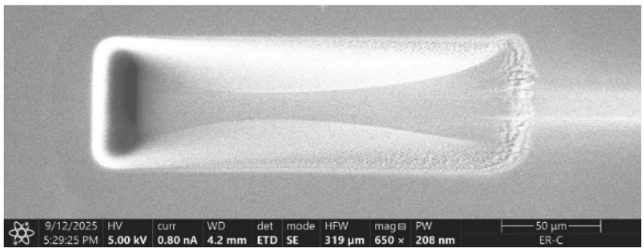

Fig. 6. Hole in a 200-µm-thick Si wafer with a 10-µm-wide PFIB W-C stripe used for this superconducting TSV.

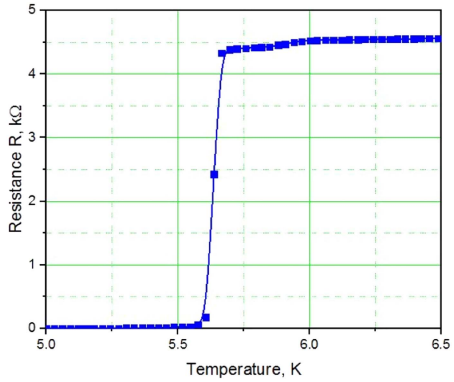

Fig. 7. *R(T)* dependence of a W-C stripe deposited with the support of Xe PFIB irradiation used for TSV with a hole in the Si wafer made by Xe PFIB etching.

deposition [23] and serve as a ground superconducting layer and/or a layer of nJJs.

IV. Conclusion

TiN films can be structured to dimensions smaller than 10 nm, and allow for the removal of HSQ resist using BHF without degradation of their superconducting properties. The use of a dirty lift-off process that limits qubit quality [24] is thereby avoided. The TiN films are O-free and more corrosion-resistant than Al, Nb and NbN films, resulting in lower losses and greater long-term stability of the nJJs. Optimization of the superconducting transition temperature, normal state resistance and critical current of TiN nJJs can be achieved by varying the deposition parameters and dimensions of the nJJs. Xe PFIB is an effective technology for the fabrication of TSVs, which promise to support the integration of TiN nJJs with superconducting and semiconducting quantum circuits. The use of a single material to form nJJs without the use of lossy dielectrics minimizes the presence of interfaces between different materials, potentially leading to higher coherence and higher quality qubits. For classical SFQ digital circuits, such junctions can be employed in multilayer integrated circuits with higher fabrication processing temperatures, leading to higher yield fabrication.

Acknowledgment

The authors gratefully acknowledge the opportunity to perform parts of the work in ER-C-1, HNF, JCNS-2, and PGI-7 at Forschungszentrum Jülich GmbH. The authors thank R. Borowski, L. Kibkalo, M. Lipińska-Chwałek, L. Risters, H. Stumpf, S. Trellenkamp, F. Lentz, S. Neduev, E. Neumann, O. Petracic, S. Nandi, B. Schmitz, and G. Potemkin for technical assistance. Views and opinions expressed are those of the author(s) only and do not necessarily reflect those of the European Union or the U.K. Science and Technology Facilities Council or the Swiss State Secretariat for Education, Research and Innovation (SERI). Neither the European Union nor the granting authorities can be held responsible for them. This work contains results obtained from experiments performed at the Ernst Ruska-Centre for Microscopy and Spectroscopy with Electrons (ER-C) at Forschungszentrum Jülich (FZJ) in Germany. ER-C beam-time access was provided via ReMade Proposal Number 34750.

References

[1] E. Angelini and B. Forgione, "IBM newsroom," Jun. 2025. Accessed: Feb. 7, 2026. [Online]. Available: https://newsroom.ibm.com/2025-06-10-IBM-sets-the-course-to-build-worlds-first-large-scale,-fault-tolerant-quantum-computer-at-new-IBM-quantum-data-center

[2] "IBM quantum, 2025 development & innovation roadmap." Accessed: Feb. 7, 2026. [Online]. Available: https://www.hpcwire.com/wp-content/uploads/2025/06/IBM-Quantum_Development-Innovation-Roadmap_2025.pdf.

[3] J. Bernhardt et al., "Quantum computer controlled by superconducting digital electronics at millikelvin temperature," 2025, arXiv:2503.09879.

[4] C. Liu et al., "Single flux quantum-based digital control of superconducting qubits in a multichip module," *PRX Quantum*, vol. 4, 2023, Art. no. 030310, doi: 10.1103/PRXQuantum.4.030310.

[5] C. E. Murray, "Material matters in superconducting qubits," *Mater. Sci. Eng.: R: Rep.*, vol. 146, 2021, Art. no. 100646, doi: 10.1016/j.mser.2021.100646.

[6] N. Missert et al., "Analysis of multilayer devices for superconducting electronics by high-resolution scanning transmission electron microscopy and energy dispersive spectroscopy," *IEEE Trans. Appl. Supercond.*, vol. 27, no. 4, Jun. 2017, Art. no. 1100704, doi: 10.1109/TASC.2017.2669579.

[7] A. Bilmes, A. K. Händel, S. Volosheniuk, A. V. Ustinov, and J. Lisenfeld, "*In-situ* bandaged Josephson junctions for superconducting quantum processors," *Supercond. Sci. Technol.*, vol. 34, 2021, Art. no. 125011, doi: 10.1088/1361-6668/ac2a6d.

[8] J. M. Martinis et al., "Decoherence in Josephson qubits from dielectric loss," *Phys. Rev. Lett.*, vol. 95, 2005, Art. no. 210503, doi: 10.1103/PhysRevLett.95.210503.

[9] M. Steffen et al., "State tomography of capacitively shunted phase qubits with high fidelity," *Phys. Rev. Lett.*, vol. 97, 2006, Art. no. 050502, doi: 10.1103/PhysRevLett.97.050502.

[10] J. Halbritter, "On the oxidation and on the superconductivity of niobium," *Appl. Phys. A*, vol. 43, pp. 1–28, 1987, doi: 10.1007/BF00615201.

[11] J. Halbritter, "ARXPS analysis and oxidation of niobium compounds," *Electrochimica Acta*, vol. 34, pp. 1153–1155, 1989, doi: 10.1016/0013-4686(89)87149-X.

[12] J. Halbritter, "Transport in superconducting niobium films for radio frequency applications," *J. Appl. Phys.*, vol. 97, 2005, Art. no. 083904, doi: 10.1063/1.1874292.

[13] R. Rodrigo, M. I. Faley, and R. E. Dunin-Borkowski, "NanoSQUIDs based on Nb nanobridges," *J. Phys.: Conf. Ser.*, vol. 1559, 2020, Art. no. 012011, doi: 10.1088/1742-6596/1559/1/012011.

[14] M. I. Faley, Y. Liu, and R. E. Dunin-Borkowski, "Titanium nitride as a new prospective material for NanoSQUIDs and superconducting nanobridge electronics," *Nanomaterials*, vol. 11, 2021, Art. no. 466, doi: 10.3390/nano11020466.

[15] M. I. Faley, H. Fiadziushkin, B. Frohn, P. Schüffelgen, and R. E. Dunin-Borkowski, "TiN nanobridge Josephson junctions and nanoSQUIDs on SiN-buffered Si," *Supercond. Sci. Technol.*, vol. 35, 2022, Art. no. 065001, doi: 10.1088/1361-6668/ac64cd.

[16] N. S. Lawand, H. van Zeijl, P. J. French, J. J. Briaire, and J. H. M. Frijns, "Titanium nitride (TiN) as a gate material in BiCMOS devices for biomedical implants," *SENSORS, 2013 IEEE*, Baltimore, MD, USA, 2013, pp. 1–4, doi: 10.1109/ICSENS.2013.6688502.

[17] M. Liu and C. T. Black, "Performance analysis of superconductor-constriction-superconductor transmon qubits," *Phys. Rev. A*, vol. 110, 2024, Art. no. 012427, doi: 10.1103/PhysRevA.110.012427.

[18] Thermo Fisher Scientific, "ChemiSTEM Technology: A revolution in EDX analytics," ChemiSTEM-Application-Brochure. Accessed: Feb. 7, 2026. [Online]. Available: https://documents.thermofisher.com/TFS-Assets/MSD/Application-Notes/ChemiSTEM-Application-Brochure.pdf

[19] H. Du, C.-L. Jia, J. Mayer, J. Barthel, C. Lenser, and R. Dittmann, "Atomic structure of antiphase nanodomains in Fe-doped $SrTiO_3$ films," *Adv. Funct. Mater.*, vol. 25, pp. 6369–6373, 2015, doi: 10.1002/adfm.201500852.

[20] K. K. Likharev, "Superconducting weak links," *Rev. Modern Phys.*, vol. 51, pp. 101–159, 1979, doi: 10.1103/revmodphys.51.101.

[21] Y. Zhang et al., "Exposure of hydrogen silsesquioxane in electron beam lithography," *Amer. Chem. Soc. Appl. Mater. Interfaces*, vol. 17, pp. 38720–38730, 2025, doi: 10.1021/acsami.5c07013.

[22] M. I. Faley, J. V. Vas, P. Lu, and R. E. Dunin-Borkowski, "NanoSQUIDs with proximity effect nanobridge Josephson junctions for future applications in electron microscopy," *IEEE Trans. Appl. Supercond.*, vol. 35, no. 5, Aug. 2025, Art. no. 1600105, doi: 10.1109/TASC.2024.3502572.

[23] J. Su, R. Boichot, E. Blanquet, F. Mercier, and M. Pons, "Chemical vapor deposition of titanium nitride thin films: Kinetics and experiments," *Cryst. Eng. Commun.*, vol. 21, pp. 3974–3981, 2019, doi: 10.1039/c9ce00488b.

[24] M. Mohseni et al., "How to build a quantum supercomputer: Scaling from hundreds to millions of qubits," 2024, *arXiv:2411.10406*.